HHS Public Access

Author manuscript

J Cell Physiol. Author manuscript; available in PMC 2024 March 13.

Published in final edited form as:

J Cell Physiol. 2021 November ; 236(11): 7578–7590. doi:10.1002/jcp.30401.

Regulatory role of TIGAR on endothelial metabolism and angiogenesis

Xiaochen He,

Heng Zeng,

Aubrey C. Cantrell,

Jian-Xiong Chen

Department of Pharmacology and Toxicology, University of Mississippi Medical Center, Jackson, Mississippi, USA

Abstract

Endothelial glycolytic metabolism plays an important role in the process of angiogenesis. TP53-induced glycolysis and apoptosis regulator (TIGAR) is a significant mediator of cellular energy homeostasis. However, the role of TIGAR in endothelial metabolism, angiogenesis, and coronary flow reserve (CFR) has not been studied. The present study investigated whether knockout (KO) of TIGAR improves endothelial glycolytic function and angiogenesis. In vitro, aortic endothelial cells (ECs) from TIGAR KO mice exhibited increased expression of 6-phosphofructo-2-kinase/fructose-2,6-bisphosphatase isoform-3 (PFKFB3) and increased glycolytic function. These were accompanied by increased mitochondrial basal/maximal respiration and ATP production. Furthermore, knockout of TIGAR in ECs enhanced endothelial proliferation, migration, and tube formation. Knockout of TIGAR also significantly increased aortic sprouting ex vivo. In vivo, knockout of TIGAR increased the expression of proangiogenic factor, angiopoietin-1 (Ang-1) in mouse hearts. Knockout of TIGAR also significantly increased coronary capillary density with enhanced CFR in these hearts. Furthermore, TIGAR KO mice subjected to pressure overload (PO), a common model to study angiogenesis and cardiac hypertrophy, exhibited elevated expression of Ang-1, VEGF, and PFKFB3 than that of the wild-type (WT) mice. WT mice subjected to PO exhibited a significant reduction of coronary capillary density and impaired CFR, but TIGAR KO mice did not. In addition, knockout of TIGAR blunted TAC-induced cardiac hypertrophy and dysfunction seen in the WT mice. In conclusion, knockout of TIGAR improves endothelial angiogenetic capabilities by enhancing the endothelial glycolytic function, mitochondrial respiration, and proangiogenic signaling, which leads to increased coronary capillary density and vascular function and protects against chronic stress.

Correspondence: Jian-Xiong Chen, Department of Pharmacology and Toxicology, University of Mississippi Medical Center, 2500 North State St, Jackson, MS 39216, USA. JChen3@umc.edu.

AUTHOR CONTRIBUTIONS

Xiaochen He, Heng Zeng, and Jian-Xiong Chen designed the research. Xiaochen He and Heng Zeng performed the research and analyzed the data. Xiaochen He and Jian-Xiong Chen wrote the paper. Xiaochen He, Aubrey C. Cantrell, and Jian-Xiong Chen revised manuscript.

CONFLICT OF INTERESTS

The authors declare that there are no conflict of interests.

SUPPORTING INFORMATION

Additional Supporting Information may be found online in the supporting information tab for this article.

Keywords

angiogenesis; cardiac hypertrophy; CFR; endothelial glycolysis; TIGAR

1 | INTRODUCTION

Endothelial cells (ECs) are one of the most abundant cell types in the heart and play a critical role in angiogenesis and myocardial perfusion (Gogiraju et al., 2019). Emerging evidence demonstrates that ECs utilize glycolysis for generating ATP (85% of the total ATP produced) rather than oxidative phosphorylation to drive sprouting, proliferation, and migration during angiogenesis (De Bock et al., 2013). Our previous studies showed that specific knockout (KO) of Sirtuin 3 (SIRT3) in ECs reduced EC glycolysis and impaired angiogenesis, and thus led to a decreased coronary flow reserve (CFR) and diastolic dysfunction (He et al., 2017). Treatment with C646, a histone acetyltransferase p300 inhibitor, improved CFR and attenuated cardiac remodeling in the SIRT3KO mice (Su et al., 2020). We and other investigators have revealed that endothelial glucose metabolism and myocardial angiogenesis play a significant role in the pathological process of cardiac hypertrophy and heart failure (HF) (Gogiraju et al., 2019; He et al., 2016, 2017, 2018; McGarrah et al., 2018; Mohammed et al., 2015; Sankaralingam & Lopaschuk, 2015; Taegtmeyer, 2004).

Glycolysis is finely tuned by 6-phosphofructo-2-kinase/fructose-2, 6-bisphosphatase isoform 3 (PFKFB3) and TP53-induced glycolysis and apoptosis regulator (TIGAR). PFKFB3 favors the synthesis of fructose 2,6-bisphosphate (F2,6-BP), a potent allosteric activator of phosphofructokinase 1 (PFK-1) (De Bock et al., 2013), and promotes glycolysis and angiogenic sprouting in ECs (De Bock et al., 2013; Schoors et al., 2014; Xu et al., 2014). In contrast, TIGAR functions as a fructose-2, 6-biphosphatase that reduces the level of F2,6-BP and inhibits glycolysis (Bensaad et al., 2006; Green & Chipuk, 2006). Up to date, the functional role of TIGAR in modulating endothelial glucose metabolism and myocardial angiogenesis has not been studied. By using the TIGAR KO mice, we aimed to explore the potential role of TIGAR in regulating endothelial metabolism and angiogenesis.

Using in vitro and ex vivo angiogenesis models, we showed that knockout of TIGAR in ECs increased expression of PFKFB3 and glycolysis together with enhanced EC migration, tube formation, and aortic sprouting. In vivo, knockout of TIGAR increased the expression of proangiogenic factor, Angiopoietin-1 (Ang-1), and significantly increased coronary capillary density and CFR in the mouse hearts. Using the pressure overload (PO)-induced myocardial angiogenesis model, we further demonstrated that knockout of TIGAR led to an elevated expression of Ang-1, VEGF, and PFKFB3. Knockout of TIGAR significantly increased myocardial capillary density and improved CFR in the mice. Our data suggest that a significant role of TIGAR in the regulation of endothelial glycolysis and myocardial angiogenesis and that it may be a novel target for the treatment of coronary vascular dysfunction.

2 | MATERIALS AND METHODS

2.1 | Mice

Male C57BL/6 mice were purchased from The Jackson Laboratory and were used as wild-type (WT) controls. Male TIGAR deficient (TIGAR KO) mice on the C57BL/6 background were kindly gifted by Dr. Jeffrey Pessin at the Albert Einstein College of Medicine and maintained in the Laboratory Animal Facilities at the University of Mississippi Medical Center (UMMC). All animals were fed laboratory standard chow and water and housed in individually ventilated cages. All protocols were approved by the Institutional Animal Care and Use Committee at UMMC (Protocol ID: 1564) and were in compliance with the National Institutes of Health Guide for the Care and Use of Laboratory Animals (NIH Pub. No. 85-23, Revised 1996).

2.2 | Primary cell culture

Mouse aortic endothelial cells (MAECs) were isolated from the WT or TIGAR KO mice ($n = 3$), as previously described with modification (Wang et al., 2016). Briefly, the WT and TIGAR KO mice were anesthetized by inhalation of 2.5% of isoflurane mixed with 100% medical oxygen in an induction chamber followed by a nose cone on a dissection pad in supine position. The depth of anesthesia was confirmed by the lack of withdrawal to toe pinch. The mice were kept warm by using a heating lamp. The abdominal and chest area were disinfected by spraying with 70% ethanol, and were opened from the midline to expose the abdominal aorta and heart. The abdominal aorta was cut at the middle to release the blood. The aorta was then flushed with 1 ml of cold phosphate-buffered saline containing 1000 U/ml of heparin via injection through left ventricular (LV). Then the thoracic aorta was quickly dissected and placed in ice-cold Dulbecco's modified Eagle's medium (Thermo Fisher Scientific) containing 1% penicillin/streptomycin in a sterile petri dish to remove surrounding adipose tissue under a microscope. The aorta was cut into 1 mm rings which were then embedded in the reduced-growth factor basement membrane matrix (ECM, Thermo Fisher Scientific) covered with endothelial growth medium (EGM-2) supplemented with growth factors and 10% fetal bovine serum in a 48-well cell culture plate. The plate was incubated at 37°C with 5% CO_2. On Day 4, the aortic segments were gently removed without damaging the growing endothelial cells and the cells were allowed to grow for an additional 2–3 days with a fresh medium. Then, the cells were trypsinized and re-plated on gelatin (0.2%, diluted from 2% stock solution, Millipore Sigma) coated 100-mm cell culture plate. The cells were incubated at 37°C with 5% CO_2 until approximately 90% confluent, and were passaged 2–3 times. Cells between Passage 4 and 10 were used for all studies. The purity of the isolated MAECs (Figure S1a) was confirmed by staining with rabbit anti-von Willebrand factor (vWF) polyclonal antibody (1:200; Santa Cruz Biotechnology) or Alexa Fluor® 488 conjugated Griffonia Bandeiraea Simplicifolia Isolectin B4 (1:50; IB4, Invitrogen).

2.3 | Metabolic assays

The oxygen consumption rate (OCR) and extracellular acidification rate (ECAR) were measured using the XF^e24 extracellular flux analyzer from Agilent Technologies, following the manufacturer's instructions and our previous studies (He et al., 2017, 2018; Zeng et

al., 2020). Briefly, cells were seeded at the density of 20,000 cells per well 1 day before the assay. The next day, the cells were washed and incubated in unbuffered assay medium supplemented with the following substrates at 37°C in a non-CO_2 incubator for 1 h. The glycolysis stress test used an assay medium supplemented with glutamine (2 mM). ECARs were measured with injections of glucose (10 mM), oligomycin (1 μM), and 2-deoxyglucose (2-DG, 100 mM). The cellular mitochondrial stress test used an assay medium containing glucose (10 mM), pyruvate (1 mM), and glutamine (2 mM). OCRs were measured with injections of oligomycin (1 μM), cyanide p-trifluoromethoxy-phenylhydrazone (FCCP, 1 μM), and rotenone/antimycin A (Rot/AA, 0.5 μM). All of the concentrations indicated above are final concentrations in the assay medium. After each assay, the cell nuclei were stained with 4′,6-diamidino-2-phenylindole to count the total number of cells per well for data normalization. The data were expressed as OCR or ECAR/10000 cells.

2.4 | Cell proliferation assay

WT and TIGAR KO MAECs were seeded at 8×10^3 cells/well in a 96-well plate and cultured for 24 h. The 3-(4,5-dimethyl-2-thiazolyl)-2,5-diphenyl-2H-tetrazolium bromide (MTT) assay (11465007001; Roche Diagnostics) was performed according to the manufacturer's instructions. Absorbance was measured at 562 nm (reference 750 nm). Cell viability was expressed as fold change as calculated by Absorbance of TIGAR KO MAEC/Average absorbance of WT MAEC.

2.5 | Glucose uptake assay

Uptake of 2-deoxyglucose was measured in the WT and TIGAR KO MAEC by using a glucose uptake-Glo™ assay kit (Promega) and luminescence intensity (relative light unit, RLU) was measured according to the manufacturer's instructions. Glucose uptake was expressed as fold change as calculated by RLU of TIGAR KO MAEC/Average RLU of WT MAEC.

2.6 | Mouse aortic ring sprouting assay

Ex vivo angiogenesis was evaluated by using isolated mouse aortas as described previously with modification (Chen & Stinnett, 2008; Chen et al., 2006, 2007; He et al., 2017; Zeng et al., 2014). Briefly, one aortic ring was placed in a well of a 96-well culture plate covered with a total of 80 μl of ECM gel. Vessel outgrowth was examined on Day 5 using an inverted microscope (AMG, Life Technologies). Quantification of vessel sprouting was performed by measuring the relative area of aortic explants outgrowth using ImageJ software.

2.7 | Tube formation assay

The tube formation assay was performed as previously described with minor modifications (Chen et al., 2004). Briefly, ECs (1×10^4 cells/well) were seeded into a 96-well plate pre-coated with 40 μl ECM gel and incubated in a regular incubator at 37°C with 5% CO_2 for 24 h. Photos of tube-like structures were captured with an AMG inverted phase-contrast microscope (AMG, Life Technologies). The numbers of branching points and segments were quantified by NIH ImageJ software with an angiogenesis analyzer plug-in (written

by Gilles Carpentier, http://image.bio.methods.free.fr/ImageJ/?Angiogenesis-Analyzer-for-ImageJ).

2.8 | Wound scratch migration assay

Wound scratch migration assays were performed as previously described (He et al., 2017; Justus et al., 2014). Briefly, 5×10^4 cells per well were seeded in a 24-well plate. A scratch wound was applied on a confluent monolayer of MAECs using a 10 μl pipette tip, and then photos were taken at T_0 using an inverted phase-contrast microscope. The cells were incubated at 37°C with 5% CO_2 for 12 h and photographed (T12). The area of the initial scratch and the area covered by the migrated cell was measured with ImageJ software, and the ratio of the two areas is the percentage of migration.

2.9 | Transverse aortic constriction procedure

WT and TIGAR KO mice (16–20 weeks of age) were subjected to PO-induced heart failure induced by transverse aortic constriction (TAC) for 8 weeks as previously described with minor modification (Tavakoli et al., 2017; Zeng et al., 2020). Briefly, the mice were anesthetized with a single intraperitoneal injection of ketamine (50 mg/kg) and xylazine (10 mg/kg), and successful anesthesia was confirmed by lack of reflex to toe pinching. The hair was then removed in the neck and chest area by using a topical depilatory agent. Sterile surgical technique was used throughout the procedures. The mice were placed in a supine position on a heating pad to keep the body temperature at 37°C. An approximately 10 mm longitudinal midline cervical incision was made to expose the proximal portion of the sternum. Partial thoracotomy to the second rib was performed under a surgical microscope and the sternum was retracted using a chest retractor. After gentle separation of the thymus and fat tissue from the aortic arch, a small piece of 6-0 silk suture was placed between the innominate and the left common carotid arteries. A small L-shaped piece of a blunt 27-gauge needle was placed parallel to the transverse aorta. The suture was tied snugly and quickly, and the needle was promptly removed to yield a constriction of 0.4 mm in diameter. The thorax was then closed using a 6-0 silk suture and mice recovered in a warming chamber until they were fully awake. The sham procedure is identical, except without the ligation of the aorta. Mice were inspected daily, and postoperative analgesia is administrated by intraperitoneal injection of 1 ml/kg body weight Carprofen (5 mg/ml) every 24 h over 3 days. An echocardiogram was conducted on mice at 8 weeks postsurgery. The animals were then euthanized, and the tissues were harvested for further experiments.

2.10 | Echocardiography

Transthoracic echocardiograms were performed on mice using a Vevo 3100 Preclinical Imaging Platform equipped with an MX400 transducer (FUJIFILM Visual Sonics Inc.). The mice were anesthetized by inhalation of 1%–1.5% isoflurane mixed with 100% medical oxygen, and the heart rate was maintained between 450 and 500 beats per minute. To assess the systolic function, M-mode cine loops were recorded and analyzed by Vevo LAB software (FUJIFILM Visual Sonics Inc.) to measure ejection fraction (EF%) and fractional shortening (FS%), (He et al., 2016; Tao et al., 2017; Zeng et al., 2020).

CFR was assessed by PW Doppler at the left proximal coronary artery (LCA) in a modified parasternal LV short-axis view. Briefly, baseline (1% isoflurane) and hyperemic (2.5% isoflurane) coronary blood flow velocity were recorded and the CFR was calculated as the ratio of hyperemic peak diastolic flow velocity to baseline peak diastolic flow velocity (He et al., 2016, 2017, 2018; Tao et al., 2017; Zeng et al., 2020).

2.11 | Histology and immunofluorescence

Cryostat sections (10-μm thickness) of the left ventricle were stained with Alexa Fluor™ 488 conjugated wheat germ agglutinin (WGA; Invitrogen) or IB4 to evaluate the size of cardiomyocyte and cardiac hypertrophy or capillary density, respectively. Microscopic photos of 5–10 fields per section per mouse were taken by using the Nikon Eclipse 80i microscope, coupled with an X-Cite® 120 Fluorescence Illumination system (Nikon Instruments). The cross-sectional area of cardiac myocyte and the number of capillaries/100 nuclei were measured by ImageJ software.

2.12 | Immunoblot analysis

Protein extractions from heart ventricular samples or cultured MAECs were prepared in lysis buffer with protease/phosphatase inhibitor cocktail (A32961, Thermo Fisher Scientific). Lysates were separated by sodium dodecyl sulfate-polyacrylamide gel electrophoresis under reducing conditions, transferred to a polyvinylidene difluoride (PVDF) membrane, and analyzed by immunoblotting. The PVDF membranes were probed with primary antibodies against Angiopoietin-1 (Ang-1, A0604; Sigma-Aldrich), VEGF (sc-507; Santa Cruz), PFKFB3 (ab181861; Abcam), β-myosin heavy chain (β-MHC, ab15; Abcam), TIGAR (sc-67273; Santa Cruz), GAPDH (#2118; Cell Signaling), or β-tubulin (#86298; Cell Signaling). The membranes were then washed and incubated with an antirabbit (31460) or antimouse (31430) secondary antibody conjugated with horseradish peroxidase (1:10,000; Thermo Fisher Scientific). Densitometries were analyzed in the Image Lab software 6.0 (Bio-Rad).

2.13 | Statistical analysis

Data are presented as mean ± *SEM*. The assumptions of normality in both comparison groups were determined by normality and the long-normality test. Statistical significance was determined by using Student's *t*-test (two-tailed) between the means of two groups, or two-way analysis of variance in the mixed-effects model followed by Dunnett post-hoc test for multiple comparisons in GraphPad Prism 8 software. $p < .05$ was considered statistically significant.

3 | RESULTS

3.1 | Knockout of TIGAR increases glycolysis and mitochondrial respiration in cultured ECs

To investigate the role of TIGAR in ECs, we first isolated the ECs from the aortas of WT and TIGAR KO mice. The isolated ECs were cultured and confirmed by staining with EC markers von Willebrand factor (vWF) and Isolectin B4 (Figure S1a). The expression of TIGAR was absent in the TIGAR KO ECs, while the expression of PFKFB3 was

significantly increased (Figure S1b), suggesting that loss of TIGAR may impact endothelial glycolytic function.

We then examined whether the loss of TIGAR affected endothelial glycolysis. The knockout of TIGAR in ECs led to a significant upregulation of basal glycolysis, glycolytic capacity, and glycolytic reserve when compared to the WT ECs (Figure 1a–d), as measured by the ECAR. This was associated with a significant increase in mitochondrial basal/maximal respiration and ATP production (Figure 1f–i). Surprisingly, glucose uptake was not significantly different between the WT and TIGAR KO ECs (Figure 1e). These data suggest that knockout of TIGAR promotes endothelial glycolysis by upregulating PFKFB3 and increases ATP production via enhancing mitochondrial respiration.

3.2 | Knockout of TIGAR increases EC angiogenesis and aortic sprouting

Since knockout of TIGAR improves EC glycolysis and that glycolysis is the main drive for angiogenesis, we further investigated whether the ablation of TIGAR promotes the angiogenesis of ECs. Tube formation was increased in the ECs of TIGAR KO mice when compared to the ECs of WT mice, as evidenced by the increased total length of the tube-like structure and the number of segments and junctions (Figure 2a–d). The MTT assay demonstrated that TIGAR KO MAECs exhibited a higher proliferation rate than the WT ECs (Figure 2e, fold change: 1.38 ± 0.08 vs. 1.00 ± 0.01). Moreover, the ECs of TIGAR KO mice exhibited a significantly higher rate of migration than the ECs of WT mice (Figure 2f). In addition, the vessel explant sprouting study demonstrated a significant increase in the vessel explant sprouting area in the TIGAR KO as compared to the vessel explants of WT mice (Figure 2g).

3.3 | Knockout of TIGAR increases capillary density and coronary flow reserve in mouse hearts

Since knockout of TIGAR improves endothelial angiogenic capabilities in cell or tissue culture, we further examined whether this would lead to increased capillaries in the mouse hearts. As shown in Figure 3a, the expression of TIGAR was absent in the heart. The basal level of Ang-1 was significantly increased in the TIGAR KO versus the WT mice, whereas the expression of VEGF was similar between the WT and TIGAR KO mice (Figure 3a), suggesting that knockout of TIGAR is more intended to promotes vessel maturation than promoting new vessel formation in normal hearts. Measurement of the capillary density by using isolectin B4 staining showed that myocardial capillaries were significantly increased in the TIGAR KO mice when compared with the WT mice (Figure 3b). Interestingly, there was no difference in the arteriole density (Figure 3c). Measurement of the coronary flow velocity by Doppler showed that the basal level of CFR was also significantly higher in the TIGAR KO mice (Figure 3d), suggesting the knockout of TIGAR improved the basal coronary microvascular function.

3.4 | Knockout of TIGAR increases capillary density and coronary flow reserve under chronic stress

TAC-induced pressure overload is a widely used method to induce myocardial angiogenesis, hypertrophy, and HF in mice (deAlmeida et al., 2010; Shiojima et al., 2005). To investigate

the role of TIGAR in myocardial angiogenesis, WT and TIGAR KO mice were subjected to TAC for 8 weeks. We then examined the levels of proangiogenic factors and myocardial angiogenesis. As shown in Figure 4a, the expression of TIGAR was absent in the heart. The level of Ang-1 and VEGF was significantly increased in the TIGAR KO when compared with the WT mice (Figure 4a), suggesting that knockout of TIGAR stabilizes the vasculature and promotes new vessel formation in the stressed hearts. This was associated with an increased expression of PFKFB3, suggesting that glycolysis might be upregulated in the TIGAR KO hearts. Loss of capillary or microvascular rarefaction is one of the key contributors to the development of coronary microvascular dysfunction (CMD), therefore, we further examined the capillary density in hearts subjected to TAC by using isolectin B4 staining. Indeed, the capillary density was also significantly increased in the TIGAR KO mice (Figure 4b). CFR is an essential predictor of cardiovascular diseases. An impaired CFR is strongly correlated with higher mortality in patients with hypertension. As shown in Figure 4c, WT mice subjected to TAC exhibited a significantly reduced CFR when compared with the TIGAR KO mice, indicating the development of CMD in the WT mice during PO-induced HF.

3.5 | Knockout of TIGAR attenuates cardiac hypertrophy and dysfunction

Given that the impaired myocardial angiogenesis and CFR contribute to the transition from adaptive to maladaptive cardiac remodeling. We then investigated the effect of TIGAR knockout on cardiac hypertrophy. The ratio of heart weight to tibia length was significantly increased in the WT mice subjected to TAC (Figure 4d). Immunoblot also showed that the expression of μ-MHC was significantly upregulated in the WT mice as compared with TIGAR KO mice subjected to TAC (Figure 4a). WGA staining revealed a significant increase in the cross-sectional area of cardiomyocytes after TAC in the WT mice than that of the TIGAR KO mice (Figure 4e). In addition, the LV mass measured by echocardiography was significantly increased in the WT mice subjected to TAC, but not in the TIGAR KO mice (Figure 4f).

Imbalance of pathological hypertrophy and angiogenesis can cause contractile dysfunction, we then measured the systolic function (Figure 4f). The EF and FS have significantly decreased in both WT and TIGAR KO mice at 8 weeks after TAC when compared to their baselines. However, the TIGAR KO mice subjected to TAC had significantly better systolic function than that of the WT mice + TAC. These data suggest that knockout of TIGAR-mediated angiogenesis that rebalances cardiac hypertrophy, at least partially, provides protective effects against PO-induced chronic stress.

4 | DISCUSSION

In the present study, for the first time, we demonstrate that knockout of TIGAR promotes endothelial glycolysis and myocardial angiogenesis, and improved CFR at normal and stressed conditions, associated with increased proangiogenic signaling as evidenced by elevated expression of Ang-1, VEGF, and PFKFB3. In addition, knockout of TIGAR blunted TAC-induced cardiac hypertrophy and dysfunction seen in the WT mice that is associated with rebalancing the coronary angiogenesis with tissue growth.

Hypertension or aortic valvular stenosis-related PO is the most common cause of HF (Okawa et al., 2019), but the underlying mechanisms remain poorly understood. The failing heart is more dependent on glycolysis for generating ATP (McGarrah et al., 2018; Sankaralingam & Lopaschuk, 2015; Wende et al., 2017), due to decreases in fatty acids and glucose oxidation (Doenst et al., 2013; Taegtmeyer, 2004). With further progression of HF, inadequate compensation by glycolysis leads to energy deficits, and increasing glycolysis can ultimately lead to substrate depletion (Nascimben et al., 2004; Neubauer, 2007). A recent study demonstrated that PO induced the level of TIGAR in the heart and that the ablation of TIGAR in cardiomyocytes preserved cardiac glucose oxidation and glycolysis during HF (Okawa et al., 2019). Our recent study also demonstrated high glucose (HG) induced the expression of TIGAR in H9c2 cells, whereas increased PFKFB3 expression and glycolysis under hyperglycemic conditions (Li et al., 2021). However, the role of TIGAR in endothelial metabolism and the exact molecular mechanism is unknown. ECs are one of the most abundant cell types in the heart and play a critical role in coronary angiogenesis, cardiac vascularization, and perfusion during physiological and pathological hypertrophy (Gogiraju et al., 2019). Although the molecular mechanisms underlying the impaired cardiac vascularization during pathological hypertrophy and HF are incompletely understood, endothelial metabolism is considered one of the major components. ECs generate most ATP through glycolysis to drive vessel sprouting, proliferation, and migration (De Bock et al., 2013). While quiescent ECs already have much higher glycolysis than cardiomyocytes, glycolytic flux can be further enhanced when ECs are activated, in part by upregulating the expression of PFKFB3 (De Bock et al., 2013; Eelen et al., 2015). In contrast, TIGAR inhibits glycolysis by decreasing the products of PFKFB3. Therefore, we hypothesized that knockout of TIGAR may enhance the endothelial glycolysis and subsequent angiogenic function.

To test whether knockout of TIGAR improves glycolysis and angiogenesis, we isolated the MAECs from both WT and TIGAR KO mice and performed metabolic and angiogenic analysis. Extracellular flux analysis demonstrates that glycolysis, glucose capacity, and glycolytic reserve were significantly increased in the TIGAR KO MAECs when compared to the WT MAECs. This was accompanied by an increase in the expression of PFKFB3. In addition, mitochondrial respiration and related ATP production were also elevated in the TIGAR KO mice, providing more energy for normal cellular function. Consistent with previous studies (Chung et al., 2004; De Bock et al., 2013; He et al., 2017, 2018), the present study revealed that the enhanced endothelial glycolysis in the TIGAR KO MAEC is associated with increased tube formation, migration, and vessel sprouting. Consistent with these results, the capillary density was increased in the normal TIGAR KO mice as compared to the WT mice, as well as the CFR, suggesting that knockout of TIGAR also improves the development of coronary vasculature and microvascular function at normal condition. Mechanistically, the expression of Ang-1 was increased in the TIGAR KO heart, but the level of VEGF was the same, indicating that knockout of TIGAR promotes the maturation of vasculature, possibly by recruiting pericytes, rather than promoting new vessel formation in normal hearts. A better CFR or coronary microvascular function indicates that an adequate supply of oxygen and nutrient substrates may be maintained during stress.

TAC-induced pressure overload in mice is a commonly used animal model for studying the mechanisms of myocardial angiogenesis, cardiac hypertrophy, and HF. To further investigate the role of TIGAR in angiogenesis, the mice were subjected to TAC for 8 weeks. We observed a reduction in the capillary density or microvascular rarefaction in the WT hearts after PO. The level of Ang-1, VEGF, and PFKFB3 was also significantly increased in the TIGAR KO when compared with the WT mice. These data suggest that, under stress, knockout of TIGAR promotes angiogenesis and vascular maturation in the hearts, via upregulating Ang-1 and VEGF. PFKFB3 is also involved probably through pumping up glycolysis. We also found that PO gradually impaired the CFR in the WT mice over 8 weeks, but not in the TIGAR KO mice, suggesting that the ablation of TIGAR also protects the coronary vascular function. Impaired CFR will result in insufficient perfusion to meet the metabolic demand, and may lead to hypoxia in the heart and promote the transition from adaptive to maladaptive cardiac remodeling (He et al., 2016; van de Hoef et al., 2015). As a consequence, the WT mice after TAC developed more severe cardiac hypertrophy and systolic dysfunction than that of the TIGAR KO mice. Since CFR reflects the function of all coronary vessels, improvement of coronary artery or microcirculation (capillaries) would lead to enhanced CFR (Gan et al., 2013). In the present study, preserving CFR and capillary density by ablation of TIGAR could partly explain the amelioration of cardiac dysfunction and hypertrophy in the TIGAR KO mice after TAC. Recent studies demonstrate that CMD plays a detrimental role in HF patients (Borlaug et al., 2010; Farrero et al., 2014). Patients with congestive heart failure have been reported to have reduced CFR (Neishi et al., 2005), suggesting a significant role of coronary microvascular function in maintaining normal cardiac function. CFR is a significant and independent determinant of long-term cardiovascular events and a predictor of cardiovascular diseases (Murthy et al., 2011; Nakanishi et al., 2012). Our findings merit further studies to find novel therapeutic targets that can rescue the impaired CFR and ameliorate the outcome of HF.

Compiling evidence suggests that EC/cardiomyocyte communication plays an important role in maintaining vascular and cardiac function. Cardiomyocytes release regulatory proteins such as Ang-1 and VEGF to promote angiogenesis and maintain coronary vessel homeostasis (He et al., 2016, 2019; Leucker et al., 2011; Lim et al., 2015; Wan & Rodrigues, 2016; Zeng & Chen, 2019). Consistent with these studies, in the TIGAR KO mice, the levels of Ang-1 and VEGF were significantly higher than that of WT mice after PO-induced hypertrophy, suggesting that the ablation of TIGAR could attenuate PO-induced impairment of angiogenic signaling. Decreased level of Ang-1 could lead to pericyte detachment, death, and subsequent vascular destabilization and loss of capillaries. These abnormalities may result in microvascular dysfunction, such as increased vascular permeability. On the other hand, coronary angiogenesis was impaired in the later phase of the development of cardiac hypertrophy and HF (Shiojima et al., 2005). Disruption of coordinated cardiac hypertrophy and angiogenesis has been shown to accelerate contractile dysfunction and the transition to HF (Shiojima et al., 2005). In our mouse model, severe cardiac dysfunction developed only in the WT mice that exhibited uncoupled cardiomyocyte growth and angiogenesis as a result of excessive cardiac hypertrophy, supports the notion that the imbalance of pathological hypertrophy and angiogenesis can cause systolic dysfunction and that knockout of TIGAR could rebalance of tissue growth and angiogenesis.

This study had some potential limitations. First, we used global TIGAR KO mice, thus other cell types (such as cardiomyocytes and smooth muscle cells (SMCs)) may also contribute to the development of microvascular rarefaction and vascular dysfunction. A previous study by Okawa et al. (2019) reported that cardiac-specific TIGAR KO mice were protected from PO-induced HF. However, their study did not investigate the role of cardiac TIGAR in angiogenesis and vascular function. Our recent study demonstrated that knockdown of TIGAR in H9c2 cells rescued HG-induced reduction of VEGF expression and improved endothelial angiogenesis in H9c2 conditioned medium (Li et al., 2021), suggesting that cardiomyocyte TIGAR can regulate the cardiac angiogenic process. SMCs regulate macrovascular (artery and arteriole) function. SMCs may also contribute to the formation of perivascular fibrosis since we did observe increased perivascular fibrosis (data not shown) in the WT mice after TAC, but not in the TIGAR KO mice. Therefore, we believed that TIGAR in SMCs may also contribute to impaired CFR. Nonetheless, the present study suggests a critical role of TIGAR in the regulation of EC glycolysis and angiogenesis, which, at least in part, contributes to the functional and metabolic changes. Further studies are needed to explore the mechanisms by which TIGAR regulates EC glycolysis and angiogenesis, as well as vascular and cardiac function by using endothelial-specific TIGAR KO mice. Vascular function and angiogenesis in the endothelial-specific TIGAR KO mice may be still protected from pressure overload, but to a lesser extent since the other cells (cardiomyocyte, smooth muscle cells, etc.) may still have impaired metabolism and function to support ECs due to the presence of TIGAR. And vice versa, cardiomyocytes may function better due to healthier EC and capillaries that provide more oxygen and nutrients than that in the WT mice.

For CFR measurement, we used 2.5% isoflurane as a vasodilator to induced hyperemia in mice, which is an effective and noninvasive method for assessing CFR in animal studies. Although the exact mechanism of isoflurane-induced vasodilation is unknown, isoflurane-mediated vasodilation is vascular smooth muscle and endothelium-dependent, associated with adenosine triphosphate-sensitive potassium channels (K_{ATP} channels) (Cason et al., 1994; Constantinides & Murphy, 2016; Gamperl et al., 2002; Zhou et al., 1998). Adenosine was also used as a vasodilator in other studies in which adenosine stimulates the release of nitric oxide (NO) or activates the adenylate cyclase-cAMP pathway to dilate coronary arteries (Hein & Kuo, 1999; Silver et al., 1984). Moreover, acetylcholine induces vasodilation via activation of endothelial NO synthase and prostaglandin (PG) production (Kellogg et al., 2005). However, its action on smooth muscle cell-mediated vasoconstriction might impede its vasodilation effect especially when endothelial dysfunction is present. In comparison between adenosine and isoflurane-induced vasodilation, You et al. (2012) suggested that although no differences were observed between the effects of adenosine and isoflurane on CFR in normal mice, using isoflurane might underestimate CFR under diseased condition. However, it is difficult to force coronary flow below a certain level for baseline measurement when using adenosine under anesthesia and thus isoflurane may be more suitable than adenosine when measuring CFR in mice (Hartley et al., 2010).

Our study demonstrated a necessary role of TIGAR in endothelial glycolytic function, angiogenesis, and coronary vascular function that may be protective against chronic stress. Mechanistically, knockout of TIGAR increased endothelial glycolysis and mitochondrial

respiration and thus promoted endothelial angiogenic signaling and capabilities. This resulted in increased expression of proangiogenic growth factors, coronary angiogenesis, and CFR, which rebalanced angiogenesis with cardiac hypertrophy and preserved cardiac function as proposed in Figure 5. The protective effect of TIGAR knockout was associated with higher levels of PFKFB3. Therefore, novel therapeutic targets that regulate endothelial metabolism, myocardial angiogenesis, and improve coronary microvascular function should be beneficial in the prevention and treatment of PO-induced hypertrophy and heart failure.

Supplementary Material

Refer to Web version on PubMed Central for supplementary material.

ACKNOWLEDGMENTS

We are very grateful to Dr. Jeffrey Pessin at the Albert Einstein College of Medicine for providing the TIGAR KO mice. We also appreciate Mr. Joshua Jefferson for the histological preparation of the tissue samples. This study was supported by the National Heart, Lung, and Blood Institute 2R01HL102042-8 and University of Mississippi Medical Center Intramural Research Support Program to Dr. Jian-Xiong Chen.

DATA AVAILABILITY STATEMENT

The data that support the findings of this study are available from the corresponding author upon reasonable request.

REFERENCES

Bensaad K, Tsuruta A, Selak MA, Vidal MN, Nakano K, Bartrons R, Gottlieb E, & Vousden KH (2006). TIGAR, a p53-inducible regulator of glycolysis and apoptosis. Cell, 126(1), 107–120. 10.1016/j.cell.2006.05.036 [PubMed: 16839880]

Borlaug BA, Olson TP, Lam CS, Flood KS, Lerman A, Johnson BD, & Redfield MM (2010). Global cardiovascular reserve dysfunction in heart failure with preserved ejection fraction. Journal of the American College of Cardiology, 56(11), 845–854. 10.1016/j.jacc.2010.03.077 [PubMed: 20813282]

Cason BA, Shubayev I, & Hickey RF (1994). Blockade of adenosine triphosphate-sensitive potassium channels eliminates isoflurane-induced coronary artery vasodilation. Anesthesiology, 81(5), 1245–1255. 10.1097/00000542-199411000-00019 [PubMed: 7978484]

Chen JX, & Stinnett A (2008). Disruption of Ang-1/Tie-2 signaling contributes to the impaired myocardial vascular maturation and angiogenesis in type II diabetic mice. Arteriosclerosis, Thrombosis, and Vascular Biology, 28(9), 1606–1613. 10.1161/ATVBAHA.108.169235 [PubMed: 18556567]

Chen JX, Lawrence ML, Cunningham G, Christman BW, & Meyrick B (2004). HSP90 and Akt modulate Ang-1-induced angiogenesis via NO in coronary artery endothelium. Journal of Applied Physiology, 96(2), 612–620. 10.1152/japplphysiol.00728.2003 [PubMed: 14555685]

Chen JX, Zeng H, Lawrence ML, Blackwell TS, & Meyrick B (2006). Angiopoietin-1-induced angiogenesis is modulated by endothelial NADPH oxidase. American Journal of Physiology: Heart and Circulatory Physiology, 291(4), H1563–H1572. 10.1152/ajpheart.01081.2005 [PubMed: 16679392]

Chen JX, Zeng H, Tuo QH, Yu H, Meyrick B, & Aschner JL (2007). NADPH oxidase modulates myocardial Akt, ERK1/2 activation, and angiogenesis after hypoxia-reoxygenation. American Journal of Physiology: Heart and Circulatory Physiology, 292(4), H1664–H1674. 10.1152/ajpheart.01138.2006 [PubMed: 17220182]

Chung SJ, Lee SH, Lee YJ, Park HS, Bunger R, & Kang YH (2004). Pyruvate protection against endothelial cytotoxicity induced by blockade of glucose uptake. International Journal of Biochemistry and Molecular Biology, 37(2), 239–245. 10.5483/bmbrep.2004.37.2.239

Constantinides C, & Murphy K (2016). Molecular and integrative physiological effects of isoflurane anesthesia: The paradigm of cardiovascular studies in rodents using magnetic resonance imaging. Frontiers in Cardiovascular Medicine, 3, 23. 10.3389/fcvm.2016.00023 [PubMed: 27525256]

De Bock K, Georgiadou M, Schoors S, Kuchnio A, Wong BW, Cantelmo AR, Quaegebeur A, Ghesquière B, Cauwenberghs S, Eelen G, Phng LK, Betz I, Tembuyser B, Brepoels K, Welti J, Geudens I, Segura I, Cruys B, Bifari F, … Carmeliet P (2013). Role of PFKFB3-driven glycolysis in vessel sprouting. Cell, 154(3), 651–663. 10.1016/j.cell.2013.06.037 [PubMed: 23911327]

deAlmeida AC, van Oort RJ, & Wehrens XH (2010). Transverse aortic constriction in mice. Journal of Visualized Experiments, 38), 1729. 10.3791/1729

Doenst T, Nguyen TD, & Abel ED (2013). Cardiac metabolism in heart failure: Implications beyond ATP production. Circulation Research, 113(6), 709–724. 10.1161/CIRCRESAHA.113.300376 [PubMed: 23989714]

Eelen G, de Zeeuw P, Simons M, & Carmeliet P (2015). Endothelial cell metabolism in normal and diseased vasculature. Circulation Research, 116(7), 1231–1244. 10.1161/CIRCRESAHA.116.302855 [PubMed: 25814684]

Farrero M, Blanco I, Batlle M, Santiago E, Cardona M, Vidal B, Castel MA, Sitges M, Barbera JA, & Perez-Villa F (2014). Pulmonary hypertension is related to peripheral endothelial dysfunction in heart failure with preserved ejection fraction. Circulation: Heart Failure, 7(5), 791–798. 10.1161/CIRCHEARTFAILURE.113.000942 [PubMed: 25047042]

Gamperl AK, Hein TW, Kuo L, & Cason BA (2002). Isoflurane-induced dilation of porcine coronary microvessels is endothelium dependent and inhibited by glibenclamide. Anesthesiology, 96(6), 1465–1471. 10.1097/00000542-200206000-00028 [PubMed: 12170061]

Gan LM, Wikstrom J, & Fritsche-Danielson R (2013). Coronary flow reserve from mouse to man--from mechanistic understanding to future interventions. Journal of Cardiovascular Translational Research, 6(5), 715–728. 10.1007/s12265-013-9497-5 [PubMed: 23877202]

Gogiraju R, Bochenek ML, & Schafer K (2019). Angiogenic endothelial cell signaling in cardiac hypertrophy and heart failure. Frontiers in Cardiovascular Medicine, 6, 20. 10.3389/fcvm.2019.00020 [PubMed: 30895179]

Green DR, & Chipuk JE (2006). p53 and metabolism: Inside the TIGAR. Cell, 126(1), 30–32. 10.1016/j.cell.2006.06.032 [PubMed: 16839873]

Hartley CJ, Reddy AK, Michael LH, Entman ML, Chintalagattu V, Khakoo AY, & Taffet GE (2010). Coronary flow reserve in mice: Effects of age, coronary disease, and vascular loading. Annual International Conference of the IEEE Engineering in Medicine and Biology Society, 2010, 3780–3783. 10.1109/IEMBS.2010.5627571 [PubMed: 21096875]

He X, Zeng H, & Chen JX (2016). Ablation of SIRT3 causes coronary microvascular dysfunction and impairs cardiac recovery post myocardial ischemia. International Journal of Cardiology, 215, 349–357. 10.1016/j.ijcard.2016.04.092 [PubMed: 27128560]

He X, Zeng H, & Chen JX (2019). Emerging role of SIRT3 in endothelial metabolism, angiogenesis, and cardiovascular disease. Journal of Cellular Physiology, 234(3), 2252–2265. 10.1002/jcp.27200 [PubMed: 30132870]

He X, Zeng H, Roman RJ, & Chen JX (2018). Inhibition of prolyl hydroxylases alters cell metabolism and reverses pre-existing diastolic dysfunction in mice. International Journal of Cardiology, 272, 281–287. 10.1016/j.ijcard.2018.08.065 [PubMed: 30177233]

He X, Zeng H, Chen ST, Roman RJ, Aschner JL, Didion S, & Chen JX (2017). Endothelial specific SIRT3 deletion impairs glycolysis and angiogenesis and causes diastolic dysfunction. Journal of Molecular and Cellular Cardiology, 112, 104–113. 10.1016/j.yjmcc.2017.09.007 [PubMed: 28935506]

Hein TW, & Kuo L (1999). cAMP-independent dilation of coronary arterioles to adenosine: Role of nitric oxide, G proteins, and K(ATP) channels. Circulation Research, 85(7), 634–642. 10.1161/01.res.85.7.634 [PubMed: 10506488]

Justus CR, Leffler N, Ruiz-Echevarria M, & Yang LV (2014). In vitro cell migration and invasion assays. Journal of Visualized Experiments: JoVE, 88, e51046. 10.3791/51046

Kellogg DL Jr., Zhao JL, Coey U, & Green JV (2005). Acetylcholine-induced vasodilation is mediated by nitric oxide and prostaglandins in human skin. Journal of Applied Physiology, 98(2), 629–632. 10.1152/japplphysiol.00728.2004 [PubMed: 15649880]

Leucker TM, Bienengraeber M, Muravyeva M, Baotic I, Weihrauch D, Brzezinska AK, Warltier DC, Kersten JR, & Pratt PF Jr. (2011). Endothelial-cardiomyocyte crosstalk enhances pharmacological cardioprotection. Journal of Molecular and Cellular Cardiology, 51(5), 803–811. 10.1016/j.yjmcc.2011.06.026 [PubMed: 21791217]

Li L, Zeng H, He X, & Chen JX (2021). Sirtuin 3 alleviates diabetic cardiomyopathy by regulating TIGAR and cardiomyocyte metabolism. Journal of the American Heart Association, 10(5), e018913. 10.1161/JAHA.120.018913 [PubMed: 33586458]

Lim SL, Lam CS, Segers VF, Brutsaert DL, & De Keulenaer GW (2015). Cardiac endothelium-myocyte interaction: Clinical opportunities for new heart failure therapies regardless of ejection fraction. European Heart Journal, 36(31), 2050–2060. 10.1093/eurheartj/ehv132 [PubMed: 25911648]

McGarrah RW, Crown SB, Zhang GF, Shah SH, & Newgard CB (2018). Cardiovascular metabolomics. Circulation Research, 122(9), 1238–1258. 10.1161/CIRCRESAHA.117.311002 [PubMed: 29700070]

Mohammed SF, Hussain S, Mirzoyev SA, Edwards WD, Maleszewski JJ, & Redfield MM (2015). Coronary microvascular rarefaction and myocardial fibrosis in heart failure with preserved ejection fraction. Circulation, 131(6), 550–559. 10.1161/CIRCULATIONAHA.114.009625 [PubMed: 25552356]

Murthy VL, Naya M, Foster CR, Hainer J, Gaber M, Di Carli G, Blankstein R, Dorbala S, Sitek A, Pencina MJ, & Di Carli MF (2011). Improved cardiac risk assessment with noninvasive measures of coronary flow reserve. Circulation, 124(20), 2215–2224. 10.1161/CIRCULATIONAHA.111.050427 [PubMed: 22007073]

Nakanishi K, Fukuda S, Shimada K, Miyazaki C, Otsuka K, Maeda K, Miyahana R, Kawarabayashi T, Watanabe H, Yoshikawa J, & Yoshiyama M (2012). Impaired coronary flow reserve as a marker of microvascular dysfunction to predict long-term cardiovascular outcomes, acute coronary syndrome and the development of heart failure. Circulation Journal, 76(8), 1958–1964. 10.1253/circj.cj-12-0245 [PubMed: 22640984]

Nascimben L, Ingwall JS, Lorell BH, Pinz I, Schultz V, Tornheim K, & Tian R (2004). Mechanisms for increased glycolysis in the hypertrophied rat heart. Hypertension, 44(5), 662–667. 10.1161/01.HYP.0000144292.69599.0c [PubMed: 15466668]

Neishi Y, Akasaka T, Tsukiji M, Kume T, Wada N, Watanabe N, Kawamoto T, Kaji S, & Yoshida K (2005). Reduced coronary flow reserve in patients with congestive heart failure assessed by transthoracic Doppler echocardiography. Journal of the American Society of Echocardiography, 18(1), 15–19. 10.1016/j.echo.2004.08.007 [PubMed: 15637483]

Neubauer S (2007). The failing heart--an engine out of fuel. New England Journal of Medicine, 356(11), 1140–1151. 10.1056/NEJMra063052 [PubMed: 17360992]

Okawa Y, Hoshino A, Ariyoshi M, Kaimoto S, Tateishi S, Ono K, Uchihashi M, Iwai-Kanai E, & Matoba S (2019). Ablation of cardiac TIGAR preserves myocardial energetics and cardiac function in the pressure overload heart failure model. American Journal of Physiology: Heart and Circulatory Physiology, 316(6), H1366–H1377. 10.1152/ajpheart.00395.2018 [PubMed: 30901275]

Sankaralingam S, & Lopaschuk GD (2015). Cardiac energy metabolic alterations in pressure overload-induced left and right heart failure (2013 Grover Conference Series). Pulmonary Circulation, 5(1), 15–28. 10.1086/679608 [PubMed: 25992268]

Schoors S, De Bock K, Cantelmo AR, Georgiadou M, Ghesquière B, Cauwenberghs S, Kuchnio A, Wong BW, Quaegebeur A, Goveia J, Bifari F, Wang X, Blanco R, Tembuyser B, Cornelissen I, Bouché A, Vinckier S, Diaz-Moralli S, Gerhardt H, … Carmeliet P (2014). Partial and transient reduction of glycolysis by PFKFB3 blockade reduces pathological angiogenesis. Cell Metabolism, 19(1), 37–48. 10.1016/j.cmet.2013.11.008 [PubMed: 24332967]

Shiojima I, Sato K, Izumiya Y, Schiekofer S, Ito M, Liao R, Colucci WS, & Walsh K (2005). Disruption of coordinated cardiac hypertrophy and angiogenesis contributes to the transition to heart failure. Journal of Clinical Investigation, 115(8), 2108–2118. 10.1172/JCI24682 [PubMed: 16075055]

Silver PJ, Walus K, & DiSalvo J (1984). Adenosine-mediated relaxation and activation of cyclic AMP-dependent protein kinase in coronary arterial smooth muscle. Journal of Pharmacology and Experimental Therapeutics, 228(2), 342–347. [PubMed: 6694113]

Su H, Zeng H, He X, Zhu SH, & Chen JX (2020). Histone acetyltransferase p300 inhibitor improves coronary flow reserve in SIRT3 (Sirtuin 3) knockout mice. Journal of the American Heart Association, 9(18), e017176. 10.1161/JAHA.120.017176 [PubMed: 32865093]

Taegtmeyer H (2004). Cardiac metabolism as a target for the treatment of heart failure. Circulation, 110(8), 894–896. 10.1161/01.CIR.0000139340.88769.D5 [PubMed: 15326079]

Tao YK, Zeng H, Zhang GQ, Chen ST, Xie XJ, He X, Wang S, Wen H, & Chen JX (2017). Notch3 deficiency impairs coronary microvascular maturation and reduces cardiac recovery after myocardial ischemia. International Journal of Cardiology, 236, 413–422. 10.1016/j.ijcard.2017.01.096 [PubMed: 28131704]

Tavakoli R, Nemska S, Jamshidi P, Gassmann M, & Frossard N (2017). Technique of minimally invasive transverse aortic constriction in mice for induction of left ventricular hypertrophy. Journal of Visualized Experiments, 127, e56231. 10.3791/56231

Van de van Hoef TP, Echavarría-Pinto M, Lavieren MA, Meuwissen M, Serruys PW, Tijssen JG, Pocock SJ, Escaned J, & Piek JJ (2015). Diagnostic and prognostic implications of coronary flow capacity: A comprehensive cross-modality physiological concept in ischemic heart disease. JACC: Cardiovascular Intervention, 8(13), 1670–1680. 10.1016/j.jcin.2015.05.032

Wan A, & Rodrigues B (2016). Endothelial cell-cardiomyocyte crosstalk in diabetic cardiomyopathy. Cardiovascular Research, 111(3), 172–183. 10.1093/cvr/cvw159 [PubMed: 27288009]

Wang JM, Chen AF, & Zhang K (2016). Isolation and primary culture of mouse aortic endothelial cells. Journal of Visualized Experiments: JoVE, 118, e52965. 10.3791/52965

Wende AR, Brahma MK, McGinnis GR, & Young ME (2017). Metabolic origins of heart failure. JACC Basic to Translation Science, 2(3), 297–310. 10.1016/j.jacbts.2016.11.009

Xu Y, An X, Guo X, Habtetsion TG, Wang Y, Xu X, Kandala S, Li Q, Li H, Zhang C, Caldwell RB, Fulton DJ, Su Y, Hoda MN, Zhou G, Wu C, & Huo Y (2014). Endothelial PFKFB3 plays a critical role in angiogenesis. Arteriosclerosis, Thrombosis, and Vascular Biology, 34(6), 1231–1239. 10.1161/ATVBAHA.113.303041 [PubMed: 24700124]

You J, Wu J, Ge J, & Zou Y (2012). Comparison between adenosine and isoflurane for assessing the coronary flow reserve in mouse models of left ventricular pressure and volume overload. American Journal of Physiology: Heart and Circulatory Physiology, 303(10), H1199–H1207. 10.1152/ajpheart.00612.2012 [PubMed: 23001834]

Zeng H, & Chen JX (2019). Microvascular rarefaction and heart failure with preserved ejection fraction. Frontiers in Cardiovascular Medicine, 6, 15. 10.3389/fcvm.2019.00015 [PubMed: 30873415]

Zeng H, He X, & Chen JX (2020). Endothelial Sirtuin 3 dictates glucose transport to cardiomyocyte and sensitizes pressure overload-induced heart failure. Journal of the American Heart Association, 9(11), e015895. 10.1161/JAHA.120.015895 [PubMed: 32468895]

Zeng H, He X, Hou X, Li L, & Chen JX (2014). Apelin gene therapy increases myocardial vascular density and ameliorates diabetic cardiomyopathy via upregulation of sirtuin 3. American Journal of Physiology: Heart and Circulatory Physiology, 306(4), H585–H597. 10.1152/ajpheart.00821.2013 [PubMed: 24363305]

Zhou X, Abboud W, Manabat NC, Salem MR, & Crystal GJ (1998). Isoflurane-induced dilation of porcine coronary arterioles is mediated by ATP-sensitive potassium channels. Anesthesiology, 89(1), 182–189. 10.1097/00000542-199807000-00025 [PubMed: 9667308]

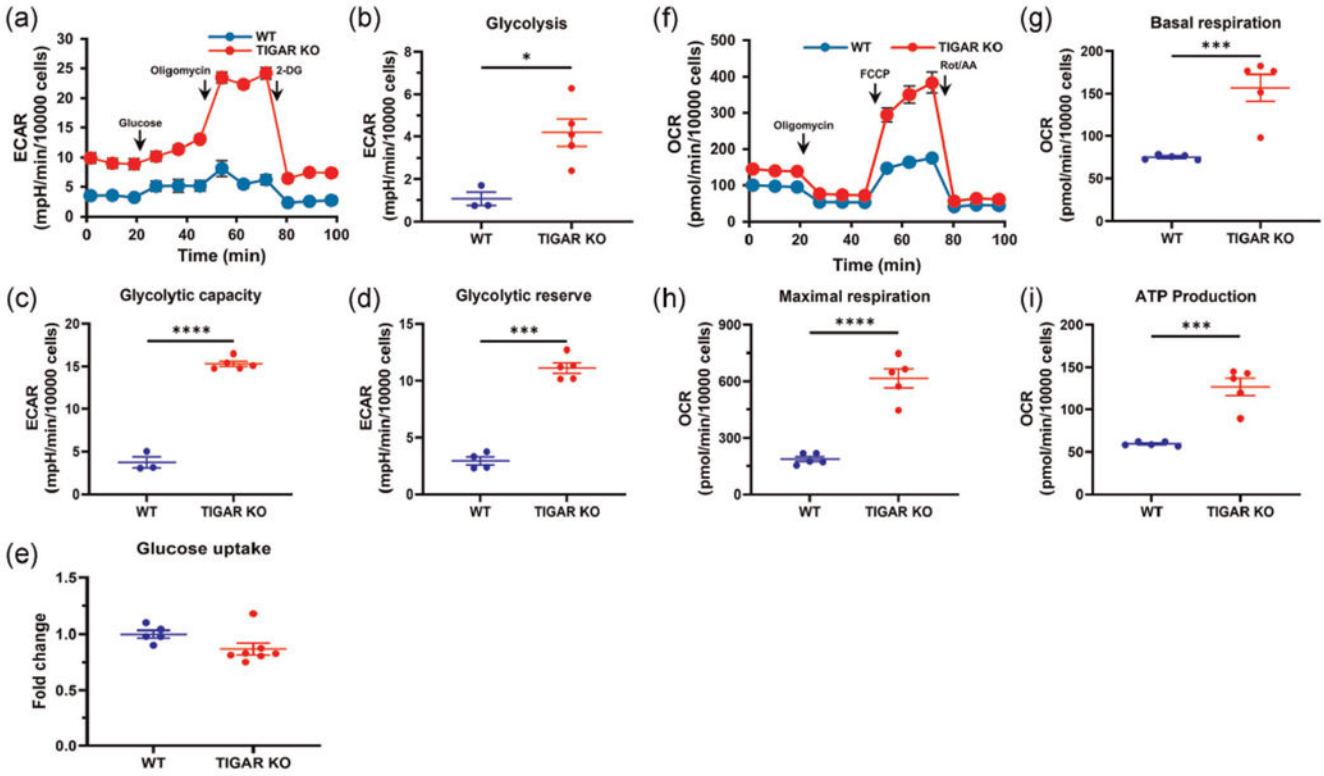

FIGURE 1.

The ablation of TIGAR increases glycolysis and mitochondrial respiration in MAEC. (a)–(d), Glycolysis stress test and extracellular flux analysis of glycolysis, glycolytic capacity, and glycolytic reserve in the MAEC isolated from TIGAR KO and WT mice (n = 3-5). (e) Glucose uptake was not different between the WT and TIGAR KO MAECs (n = 5–7). (f)–(i) Mitochondrial stress test and extracellular flux analysis of mitochondrial basal and maximal respiration and ATP production in the MAEC isolated from TIGAR KO and WT mice (n = 5). ***p < .001, ****p < .0001. KO, knockout; MAECs, mouse aortic endothelial cells; TIGAR, TP53-induced glycolysis and apoptosis regulator; WT, wild type

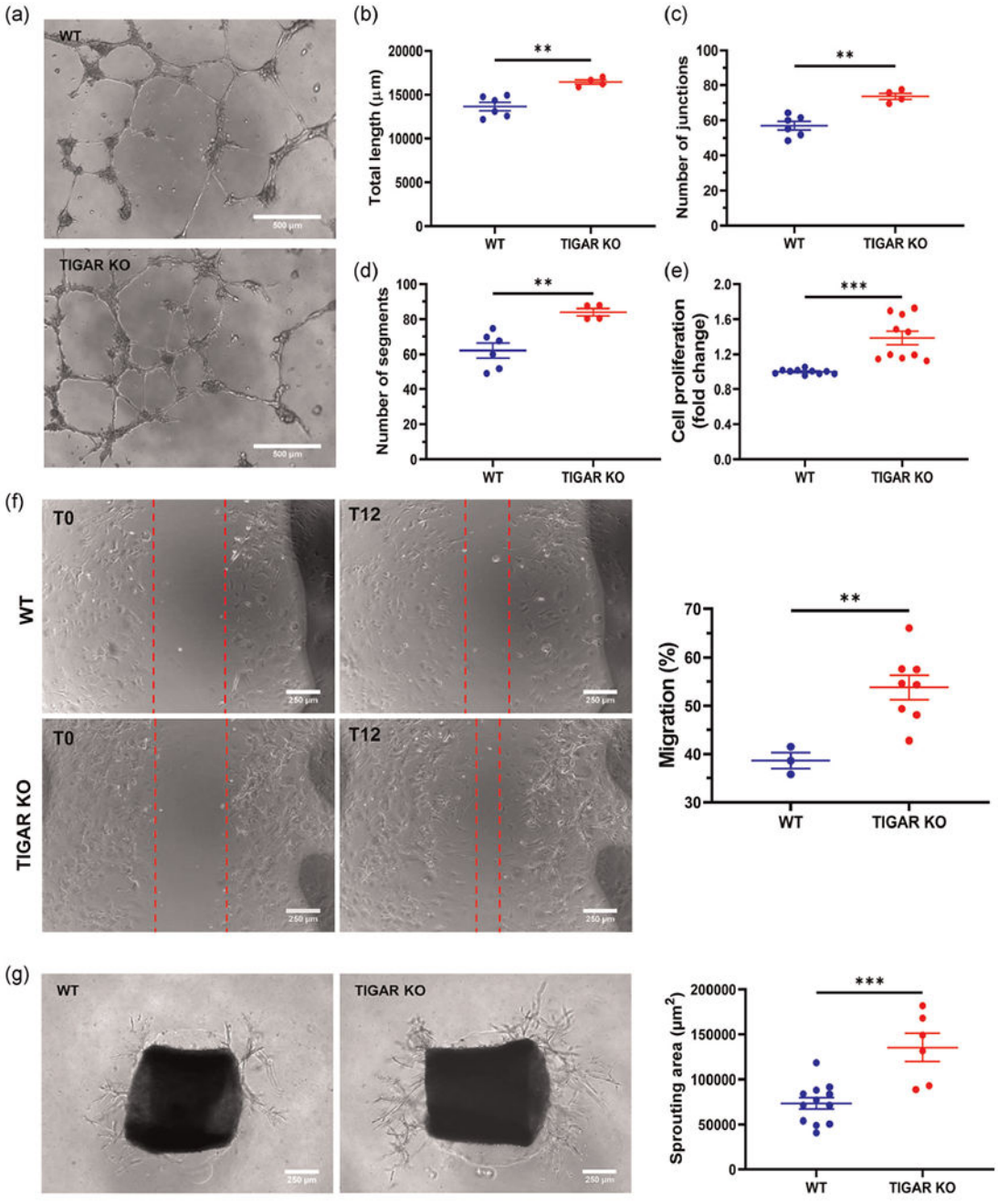

FIGURE 2.

The ablation of TIGAR increases angiogenesis of MAEC. (a)–(d) The representative images of the tube-formation assay at 12 h of incubation and quantification of the number of master segments and the total length of the tube-like structures in the indicated groups (n = 4–6). **p < .01. Bar = 500 μm. (e) Cell proliferation of TIGAR KO MAEC was significantly higher than that of the WT MAECs, as measured by MTT assay (n = 10). ***p < .001. (f) The representative images of wound scratch assay at 0 and 12 h of incubation and quantification of MAEC migration in the indicated groups (n = 3–8). **p <

.01. Bar = 250 μm. (g) The representative images of aortic ring sprouting assay at Day 5 of incubation and quantification of the sprouting area in the indicated groups (n = 6–12). Bar = 250 μm. ***p < .001. KO, knockout; MAECs, mouse aortic endothelial cells; MTT, 3-(4,5-dimethyl-2-thiazolyl)-2,5-diphenyl-2H-tetrazolium bromide; TIGAR, TP53-induced glycolysis and apoptosis regulator; WT, wild type

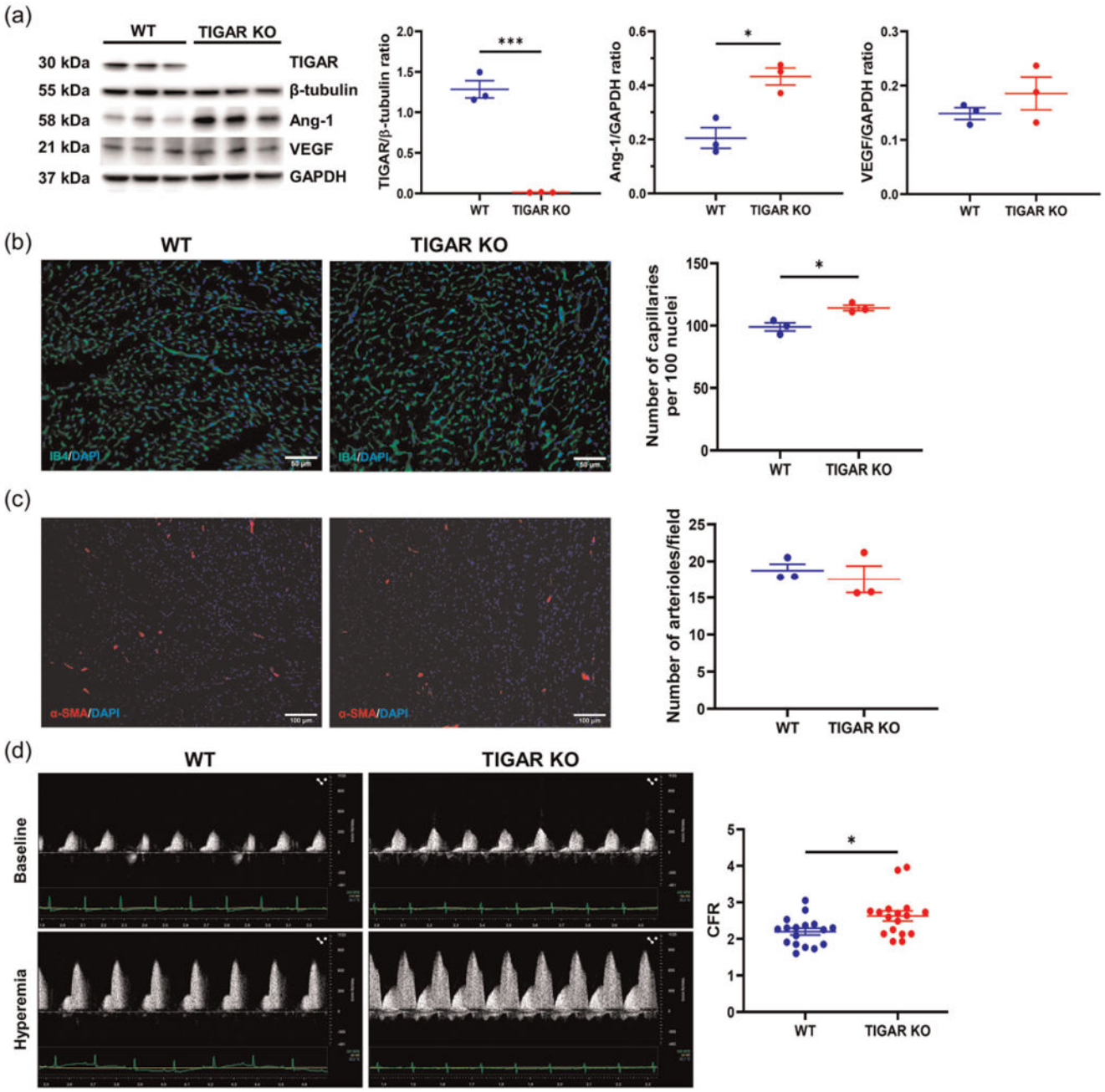

FIGURE 3.

The ablation of TIGAR increases capillary density and coronary flow reserve (CFR) in normal hearts. (a) Representative immunoblots and quantitative analysis of TIGAR, Angiopoietin-1 (Ang-1), VEGF, GAPDH, and β-tubulin in the indicated mouse hearts (n = 3). *p < .05, ***p < .001. (b) The representative images of Isolectin B4 (IB4, green; DAPI stains the nuclei, blue)-stained frozen heart sections and quantification of the number of capillaries/100 nuclei in the indicated groups (n = 3). *p < .05. Bar = 50 μm. (c) The representative images of α-smooth muscle actin (α-SMA, red; DAPI stains the nuclei, blue)-stained frozen heart sections and quantification of the number of arterioles/field in

the indicated groups ($n = 3$). (d) The representative pulsed-wave Doppler images of the proximal left coronary arteries of WT and TIGAR KO mice at 16–20 weeks of age. CFR was calculated as the ratio of hyperemic peak diastolic flow velocity (2.5% isoflurane) to baseline peak diastolic flow velocity (1% isoflurane) in the indicated groups ($n = 17$). *$p <$ .05. DAPI, 4′,6-diamidino-2-phenylindole; KO, knockout; TIGAR, TP53-induced glycolysis and apoptosis regulator; WT, wild type

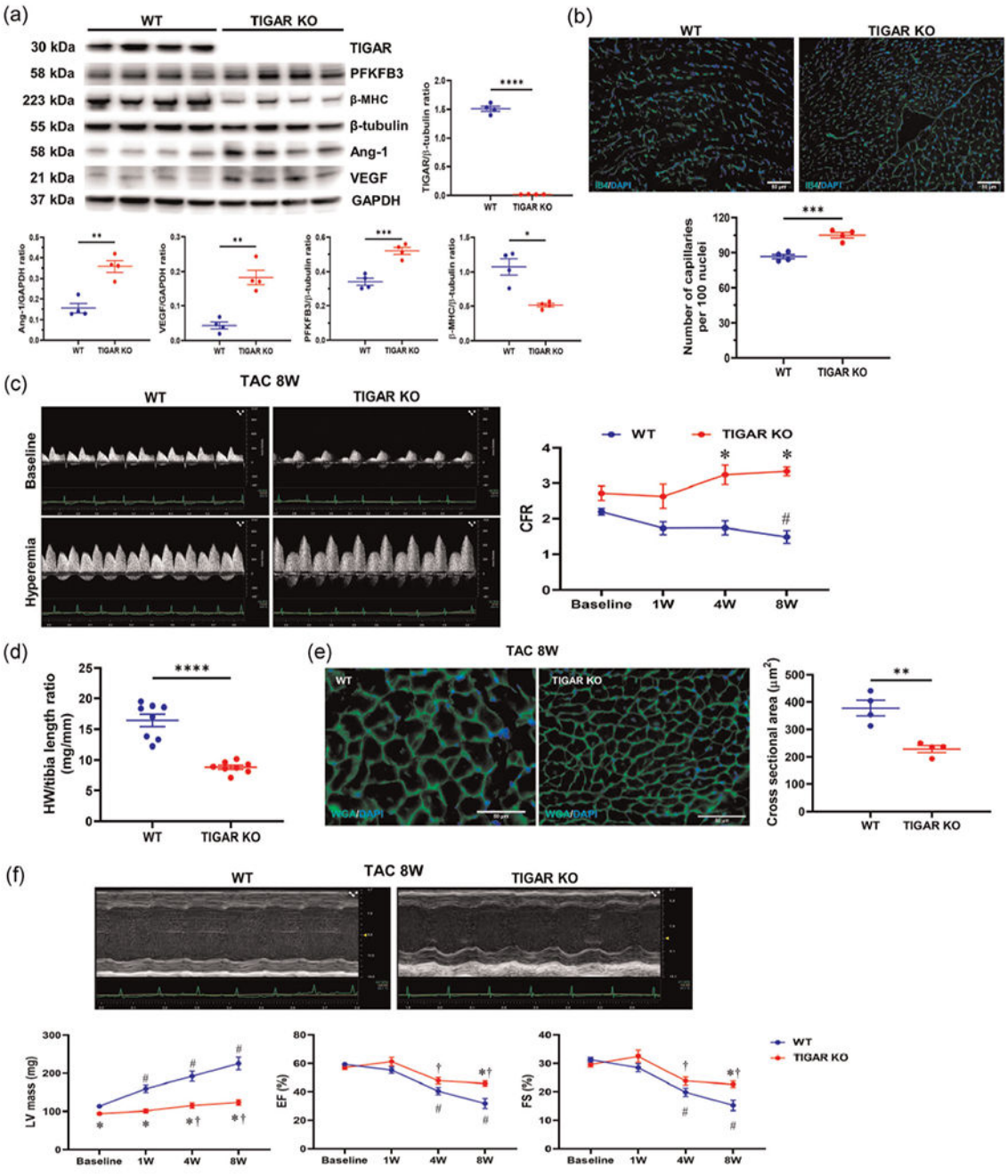

FIGURE 4.

The ablation of TIGAR increases capillary density and coronary flow reserve (CFR) and attenuated cardiac hypertrophy and dysfunction in stressed hearts. (a) Representative immunoblots and densitometry analysis of TIGAR, Ang-1, VEGF, PFKFB3, β-MHC, and corresponding GAPDH or β-tubulin in the WT and TIGAR KO mice 8 weeks after TAC surgery. $n = 4$. $^{**}p < .01$, $^{***}p < .001$, $^{****}p < .0001$. (b) The representative images of Isolectin B4 (IB4, green; DAPI stains the nuclei, blue)-stained frozen heart sections and quantification of the number of capillaries/100 nuclei 8 weeks after TAC surgery ($n = 3$).

***$p < .001$. Bar = 50 μm. (c) The representative pulsed-wave Doppler images of the proximal left coronary arteries of WT and TIGAR KO mice 8 weeks after TAC surgery. CFR gradually decreased in the WT mice, but it was not changed in the TIGAR KO mice (n = 8–18). *$p < .05$ versus corresponding WT mice, $^{\#}p < .05$ versus WT baseline. (d) Ratio of heart weight to tibia length in the WT and TIGAR KO mice 8 weeks after TAC surgery (n = 8). ****$p < .0001$. (e) The representative images of wheat germ agglutinin-stained frozen heart sections in the WT and TIGAR KO mice 8 weeks after TAC surgery. Cardiomyocyte hypertrophy is evident, as assessed by cross-sectional areas in the indicated groups. Bar = 50 μm. A minimum of 100 cardiomyocytes from each LV section of each mouse was measured (n = 4). **$p < .01$. (f) The representative echocardiographic images of WT and TIGAR KO mice subjected to TAC procedure for 8 weeks and the time course of left ventricular (LV) mass, ejection fraction (EF), and fractional shortening (FS) during the 8 weeks of pressure overload (n = 8–18). *$p < .05$ versus corresponding WT mice, $^{\#}p < .05$ versus WT baseline, $^{\dagger}p < .05$ versus TIGAR KO baseline. KO, knockout; TIGAR, TP53-induced glycolysis and apoptosis regulator; WT, wild type

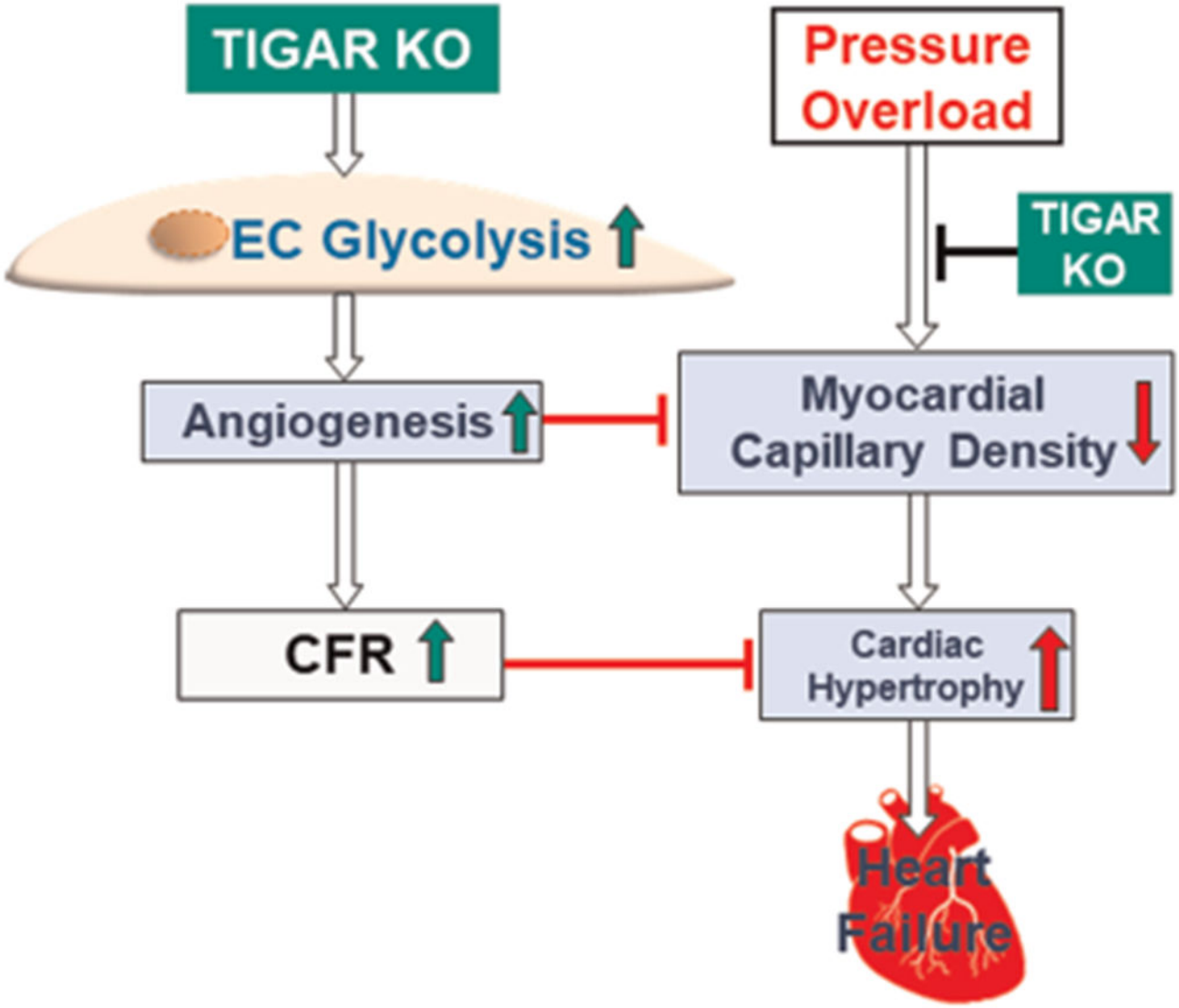

FIGURE 5.

Schematic of the proposed role of TIGAR in EC metabolism and angiogenesis. Loss of TIGAR in EC increases endothelial glucose metabolism which improves angiogenesis and coronary microvascular function and eventually blunts pressure overload-induced LV hypertrophy and heart failure. CFR, coronary flow reserve; EC, endothelial cell; KO, knockout; LV, left ventricular; TIGAR, TP53-induced glycolysis and apoptosis regulator